International Scholarly Research Network
ISRN Ceramics
Volume 2012, Article ID 854831, 10 pages
doi:10.5402/2012/854831

Research Article

Electrical Properties and AC Conductivity of $(Bi_{0.5}Na_{0.5})_{0.94}Ba_{0.06}TiO_3$ Ceramic

Ansu K. Roy,[1] Amrita Singh,[1] Karishma Kumari,[1] K. Amar Nath,[1] Ashutosh Prasad,[1] and K. Prasad[2]

[1] *University Department of Physics, T.M. Bhagalpur University, Bhagalpur 812007, India*
[2] *Centre for Applied Physics, Central University of Jharkhand, Ranchi 835205, India*

Correspondence should be addressed to Ashutosh Prasad, apd.phy@gmail.com

Received 9 August 2012; Accepted 29 August 2012

Academic Editors: H. Maiwa and J. Sheen

Lead-free perovskite $(Bi_{0.5}Na_{0.5})_{0.94}Ba_{0.06}TiO_3$ (BNBT06) was prepared by conventional ceramic fabrication technique at 1160°C/3h in air atmosphere. The crystal structure, microstructure, dielectric, polarization, piezoelectric properties, and ac conductivity of the sample were studied. X-ray diffraction data confirmed the formation of a single phase tetragonal unit cell. Williamson-Hall plot was used to calculate the lattice strain and the apparent particle size. The experimental relative density of BNBT06 was found to be ~96-97% of the theoretical one with an average grain size ~4 μm. Room temperature dielectric constant and loss factor at 1 kHz were found to be equal to 781 and 0.085, respectively. Longitudinal piezoelectric charge coefficient of the poled sample under 2.5 kV/mm at 80°C in silicone bath was found to be equal to 124 pC/N. Complex impedance and electric modulus spectroscopic analyses showed the dielectric relaxation in the material to be of non-Debye type. The Nyquist plots and conductivity studies showed the NTCR character of BNBT06. The correlated barrier hopping model (CBHM) as well as jump relaxation model (JRM) was found to successfully explain the mechanism of charge transport in BNBT06. The ac conductivity data were used to evaluate the minimum hopping length, apparent activation energy, and density of states at Fermi level.

1. Introduction

In recent years, there has been a global hunt of piezoelectric materials for their possible use in different electronic devices, and in near future a further increase in their demand is expected. In view of lead zirconium titanate, $Pb(Zr,Ti)O_3$ (PZT) containing 60–70% of lead which emanates the toxic lead oxide during calcination/sintering, attempts are being made nowadays by the European Union Governments to ban the use of lead-bearing substances harmful to the environment by way of directives like restriction of hazardous substances (RoHS) directive, the end-of-life vehicles (ELV) directive, and the waste electrical and electronic equipment (WEEE) directive [1], and so forth and other countries are following on similar lines. Therefore, there is an urgent need for novel lead-free piezoelectric solid solutions that can be used as alternatives to PZT [2]. Bismuth sodium titanate $(Bi_{0.5}Na_{0.5})TiO_3$ (BNT), belonging to the ABO_3-type perovskite family, is considered to be an excellent lead-free piezoelectric material which shows strong ferroelectric properties with rhombohedral symmetry ($R3c$) at ambient temperature having the planar electromechanical coupling factor (k_p) ~0.15, Curie temperature (T_c) at 320°C, and a remnant polarization (P_r) ~38 μC/cm^2. However, dense BNT ceramic is difficult to be prepared, requiring sintering temperatures above 1200°C, resulting in significant loss of bismuth. Besides, high leakage currents and high coercive field (~73 kV/cm) negatively affect the poling process and polarization saturation is difficult to achieve in conventionally fabricated BNT samples. In addition, BNT exhibits a low depolarization temperature ~200°C. Several workers [3–16] have investigated the electrical behavior, proposed more accurate measurement of the phase transition temperatures of BNT-based solid solutions, and determined their morphotropic phase boundary (MPB) compositions in order to improve dielectric and piezoelectric

properties of BNT ceramic. Among these solid solutions, $(Bi_{0.5}Na_{0.5})_{1-x}Ba_xTiO_3$ (BNBTx) has attracted an enormous global attention owing to the existence of a rhombohedral-tetragonal morphotropic phase boundary (MPB) near $x = 0.06 - 0.08$ in the system. Compared with pure BNT, the BNBTx ceramics have been reported to possess relatively high piezoelectric properties and low coercive field near the MPB. The study of electrical conductivity in the ferroelectric compounds is very important from the point of view that the associated physical properties like pyroelectricity, piezoelectricity, and strategy for poling are dependent on the nature and magnitude of conductivity in these materials. In this context, it would be worth mentioning that the information about the electrical properties of BNBTx is still not complete and consistent. Therefore, in order to have knowledge about the performance of BNBTx, it is important to know the carrier transport mechanism in this system and hence the system deserved further investigation. An extensive literature survey revealed that no attempt has so far been made to understand the conduction mechanism in BNBTx using impedance spectroscopy technique. It is with these views that the structural, microstructural, dielectric, polarization, piezoelectric, electric impedance, and ac conductivity studies of $(Bi_{0.5}Na_{0.5})_{0.94}Ba_{0.06}TiO_3$ (abbreviated as BNBT06) ceramic near MPB composition have been undertaken in the present work. Further, an attempt has been made to explain the conduction mechanism in BNBT06 using complex impedance and electric modulus spectroscopy techniques.

2. Experimental

Polycrystalline $(Bi_{0.5}Na_{0.5})_{0.94}Ba_{0.6}TiO_3$ ceramic was prepared by a standard high-temperature solid-state reaction technique using AR grade (purity more than 99.5%, Hi-Media) oxides and/or carbonates: Bi_2O_3, Na_2CO_3, $BaCO_3$, and TiO_2 in a suitable stoichiometry. The above ingredients were mixed thoroughly, first in air and then in methanol medium, using agate mortar and pestle. This mixture was calcined at an optimized temperature of 1160°C for about 3 hrs in an AR-grade alumina crucible. Then, by adding a small amount of polyvinyl alcohol (PVA) as binder to the calcined powder, circular and rectangular disc-shaped pellets were fabricated by applying uniaxial pressure of 6 tons/square inch. The pellets were subsequently sintered at an optimized temperature of 1180°C in air atmosphere for about 2 hrs to achieve maximum density (~97% of the theoretical density).

The X-ray diffraction (XRD) spectrum was observed on calcined powder of BNBT06 with an X-ray diffractometer (XPERT-PRO, Pan Analytical) at room temperature, using CuK_α radiation ($\lambda = 1.5405$ Å) between 2θ values of 20° and 80°. The microstructure of the sintered pellet was studied at room temperature from the micrograph obtained by using a scanning electron microscope (JEOL-JSM840A). The dielectric constant (ε), loss tangent ($\tan\delta$), electrical impedance (Z), and phase angle at different frequencies (1 Hz–1 MHz) and temperatures (20°C–450°C) were measured using a computer-controlled LCR Hi-Tester (HIOKI 3532-50, Japan) on a symmetrical cell of type Ag|ceramic|Ag, where Ag is a conductive paint coated on either side of the pellet. AC conductivity data were obtained using a relation: $\sigma_{ac} = 2\pi f \varepsilon_o \varepsilon \tan\delta$. The P-E hysteresis loop at room temperature was traced using an automatic PE-loop tracer (Marine India Electrocom Ltd., New Delhi, India). Longitudinal piezoelectric charge coefficient (d_{33}) as well as transverse piezoelectric charge coefficient (d_{31}) of the poled ceramic sample (on which a dc electric field ~2.5 kV/mm was applied by keeping it in a silicone oil bath at 80°C) was measured using PM3500 d_{33} meter (KCF Technologies, PA, USA).

3. Results and Discussion

3.1. Structural and Microstuctural Studies. Figure 1 shows the XRD spectrum of calcined BNBT06 powder at room temperature. A standard computer program (POWD) was utilized for the XRD-profile analysis. Good agreement between the observed and calculated interplanar spacing and no trace of any extra peaks due to the constituent oxides was found, thereby suggesting the formation of a single-phase compound having the tetragonal structure with lattice parameters $a = 3.8564$ Å and $c = 3.9001$ Å. The unit cell volume and tetragonality of lattice (c/a) were estimated to be ~ 58.0016 Å^3 and 1.0113, respectively. The occurrence of tetragonal nature in BNBT06, which has rhombohedral nature due to BNT phase and tetragonal nature due to barium titanate (BT), is confirmed by the splitting of peak between 46°-47° into two peaks (200) and (002). The apparent particle size and lattice strain were estimated by analyzing the X-ray diffraction peak broadening, using Williamson-Hall approach: $B\cos\theta = 2(\Delta\xi/\xi)\sin\theta + K\lambda/D$, where D is the apparent particle size, B is the diffraction peak width at half intensity, $\Delta\xi/\xi$ is the lattice strain, and K is the Scherrer constant (= 0.89). The term $K\lambda/D$ represents the Scherrer particle size distribution. The lattice strain was estimated from the slope of the plot $B\cos\theta$ as a function of $\sin\theta$ and the apparent particle size was estimated from the intersection of this line at $\sin\theta = 0$. A linear least squares fitting to $B\cos\theta/\lambda - \sin\theta/\lambda$ data provided the values of the intercept and slope of the plot. A Lorentzian model ($I = I_o + (2A/\pi)[B/\{4(\theta - \theta_c)^2 + B^2\}]$) was applied to estimate the diffraction width at half peak intensity. Here A and θ_c are the area and centre of the curve, respectively. The inset of Figure 1 illustrates the Williamson-Hall plot for BNBT06. The apparent particle size and lattice strain are estimated to be of the order of 25 nm and 0.0037, respectively.

The theoretical density for $(Bi_{0.5}Na_{0.5})_{0.94}Ba_{0.06}TiO_3$ (BNT) was calculated using the equation: $\rho = (W_1+W_2)/(W_1/\rho_1 + W_2/\rho_2)$, where W_1 and W_2 are the weight percentages of the BNT and BT in the mixture, respectively, and ρ_1 and ρ_2 are the densities of the $(Bi_{0.5}Na_{0.5})TiO_3$ (=5.32 g/cm^3) and $BaTiO_3$ (=6.02 g/cm^3), respectively. The theoretical density of BNBT06 was found to be equal to 5.357 g/cm^3. Using Archimedes principle, the apparent density of sintered ceramic was found to be equal to 5.234 g/cm^3, thereby giving the relative density of BNBT06 ~96-97% of the theoretical

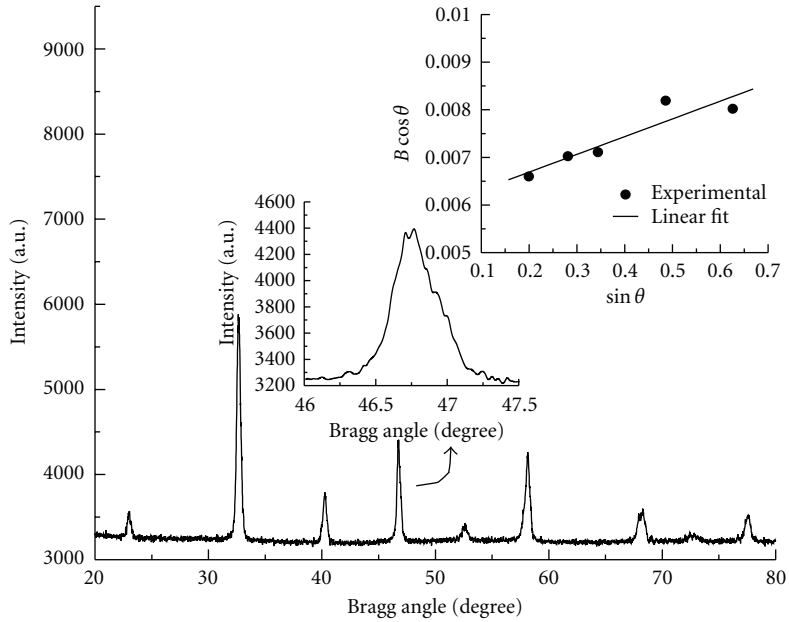

Figure 1: X-ray diffraction pattern of BNBT06 at room temperature. Inset: enlarged view of XRD pattern between 46°-47° and the Williamson-Hall plot.

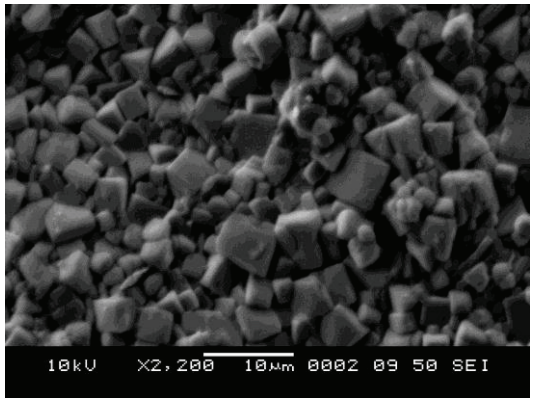

Figure 2: SEM micrograph of BNBT06 with 10 μm scale.

one. Figure 2 shows the SEM micrograph of BNBT06 with 10 μm scale. Grains of unequal sizes appear to be distributed throughout the sample. The average grain size was estimated to be about 4 μm. The ratio of average crystallite size to the grain size of BNBT06 is found to be $\sim 10^{-3}$. Also, the SEM micrograph does not seem to contain any pores or voids, thereby clearly indicating the high density of the sample.

3.2. Dielectric Studies. The frequency dependence of the dielectric constant (ε) and loss tangent (tanδ) at different temperatures are shown in Figure 3. It is observed that ε follows an inverse dependence on frequency, normally followed by almost all dielectric and/or ferroelectric materials. Dispersion with relatively high dielectric constant can be seen in the ε-f graph in the lower frequency region and dielectric constant drops at higher frequencies. The modified

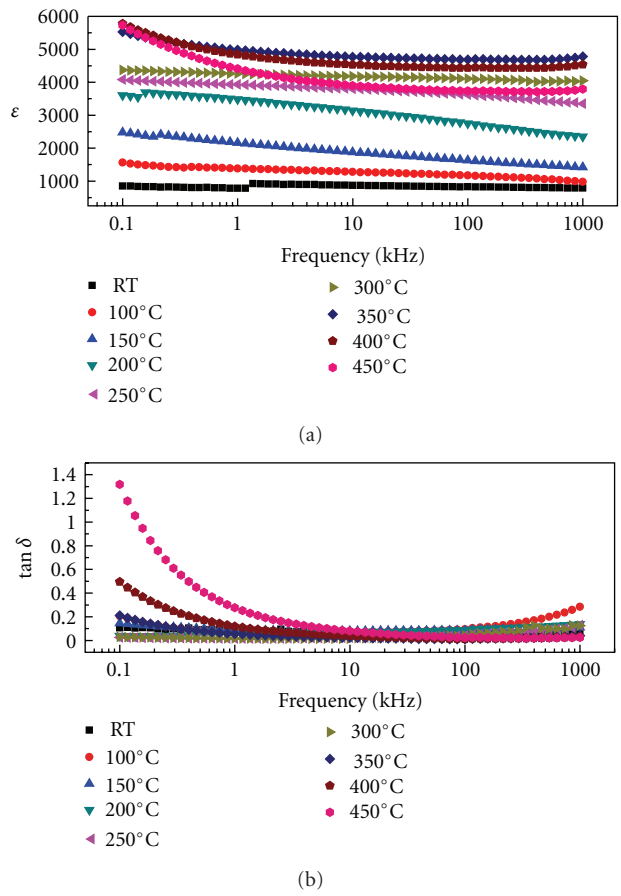

Figure 3: Variation of dielectric constant and loss tangent with frequency at different temperatures for BNBT06.

Debye equation related to a free dipole oscillating in an alternating field is expressed as $\varepsilon^* = \varepsilon_\infty + (\varepsilon_s - \varepsilon_\infty)/[1 + (i\omega\tau)^{1-\alpha}]$, where ε_s and ε_∞ are the low- and high-frequency values of ε; ω $(=2\pi f)$ is the cyclic frequency f being the frequency of measurement; τ the relaxation time; α a measure of the distribution of relaxation time. A relatively high dielectric constant at low frequencies is a characteristic of a dielectric material. At very low frequencies ($\omega \ll 1/\tau$), dipoles follow the field and we have $\varepsilon \approx \varepsilon_s$ (the value of dielectric constant at quasistatic fields). As the frequency increases ($\omega < 1/\tau$), dipoles begin to lag behind the field and hence ε slightly decreases. When the frequency reaches the characteristic frequency ($\omega = 1/\tau$), the dielectric constant drops (relaxation process) and at high frequencies ($\omega \gg 1/\tau$), dipoles are no longer able to follow the field and hence $\varepsilon \approx \varepsilon_\infty$. This behavior has been observed to be followed in case of BNBT06, at least qualitatively. The value of ε at room temperature at 1 kHz was found to be equal to 781. Further, the value of tanδ decreases with increasing frequency in the high temperature region. On the other hand, at a lower temperature, it reaches a minimum that shifts to the lower frequency side. The frequency-dependent dielectric loss of the material implies that the hopping of charge carriers plays an important role in modifying transport processes occurring in it because a loss peak is an essential feature of the charge carrier hopping transport [17]. Figure 4 shows $\varepsilon(T)$ and tanδ (T) for BNBT06 at different frequencies. It is seen from the plots that the position of the dielectric loss peak shifts to higher frequency side with increase in temperature, thereby suggesting the relaxation to be thermally activated. Further, all the plots show broad maxima (i.e., diffuse phase transition (DPT) near T_m (~350°C), where antiferroelectric to paraelectric phase transition takes place, and another maxima near depolarization temperature T_d (where ferroelectric to antiferroelectric phase transition takes place) at around 125°C. The broadening in the dielectric peak is a common feature in solid solutions, thereby indicating the presence of more than one cation in the sublattice that can produce some kind of heterogeneity. Also, almost stationary temperature-dependent loss tangent curves retain their shapes upto the transition temperature (T_m) beyond which the tanδ values sharply increase, possibly due to release of space charge polarization. Room temperature value of tanδ at 1 kHz was found to be equal to 0.085.

3.3. Hysteresis and Piezoelectric Studies. Attempts have been made to measure the electric field-induced polarization through (P-E) hysteresis loop for the virgin sample kept in silicone oil at room temperature (Figure 5). The study revealed that no saturation in polarization-electric field (P-E) curve could be obtained for the ceramic up to the maximum applied electric field due to the low resistivity of the sample. The sample could not withstand electric field beyond 1.5 kV/mm and further increase in electric field led to electrical breakdown, hence an unsaturated P-E loop for the bulk material sample. For maximum applied electric field ~1.223 kV/mm, coercivity was found to be equal to 0.815 kV/mm.

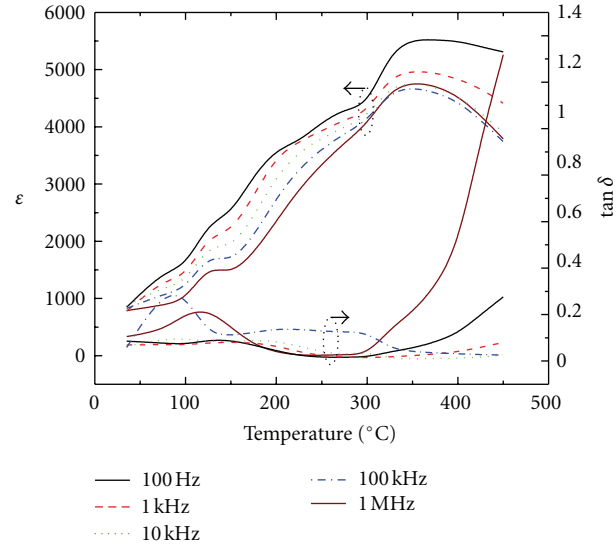

Figure 4: Temperature-dependent variation of dielectric constant and loss tangent at different indicated frequencies for BNBT06.

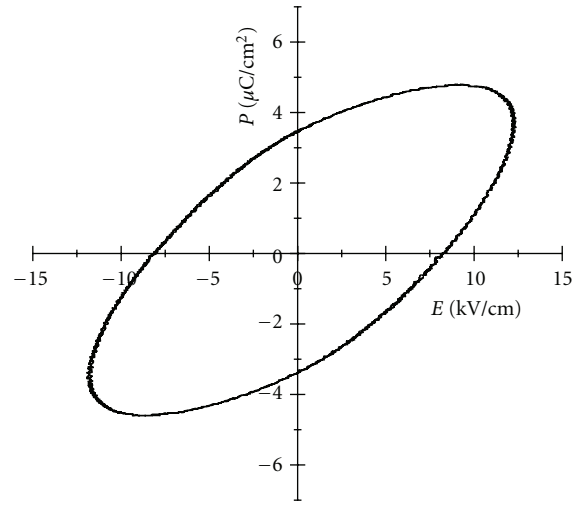

Figure 5: Room temperature P-E hysteresis loop of BNBT06 sample.

Longitudinal piezoelectric charge coefficient (d_{33}) of the poled ceramic sample was found to be equal to 124 pC/N. Such a high value of d_{33} confirmed the presence of morphotropic phase boundary (coexistence of rhombohedral and tetragonal phases) in the BNBT06 composition. However, the value of transverse piezoelectric charge coefficient d_{31} was found to be low (~12 pC/N), giving thereby the value of hydrostatic charge coefficient d_h $(= d_{33} + 2d_{31})$ equal to 148 pC/N. Due to the limiting range of measurement (which is only 5 kV) of our poling instrument and coercivity of the material used, we had to take the thickness of the samples small (~1 mm or less). Consequently, we could get only a small amount of charge accumulation on the comparatively small perpendicular surface area, thereby yielding a smaller value of d_{31} in comparison with that of d_{33}, thus causing a discrepancy. On a naïve view, this anomaly may possibly be

ascribed to the leakage of charge from the surface during manual adjustment of gap between the tips meant for d_{31} measurement in the instrument (d_{33}/d_{31} meter). However, there is every chance of creeping up of other dominating factors causing the anomaly, not known to the authors at this point of time. Things may come out only after repeating the experiments under different conditions of poling such as changing the temperature of silicone oil (normally not exceeding 100°C) and/or time of poling (normally not exceeding 30 minutes).

3.4. Electrical Impedance, Electric Modulus, and AC Conductivity Studies

3.4.1. Electrical Impedance Analysis. Complex impedance spectroscopy has been considered as a powerful non-destructive tool to study the microstructure and the electrical properties of solids, where the electrical properties are often represented in terms of some complex parameters like complex impedance $Z^*(\omega)(= Z' - jZ'' = R_s - j/\omega C_S)$; complex permittivity $\varepsilon^*(\omega)(= \varepsilon' - j\varepsilon'')$; complex electric modulus $M^*(\omega)(= M' + jM'')$; complex admittance $Y^*(\omega)(= Y' + jY'' = 1/R_p + j\omega C_p)$. They are interrelated as $M^* = 1/\varepsilon^* = j\omega C_o Z^* = j\omega C_o(1/Y^*)$ and the loss tangent, $\tan\delta = \varepsilon''/\varepsilon' = Z'/Z'' = M''/M'$, where R_s, C_s are the series resistance and capacitance; R_p, C_p are the parallel resistance and capacitance, respectively. It is known that for Debye-type relaxation, one expects semicircular Argand (Cole-Cole or Nyquist) plots with the centre located on the z'-axis. On the other hand for a non-Debye-type relaxation, these Argand complex plane plots are close to semicircular arcs with endpoints on the real axis and the center lying below the abscissa. The complex impedance in such a case can be described as $Z^*(\omega) = Z' + iZ'' = R/[1 + (i\omega/\omega_o)^{1-\alpha}]$, where α, as referred to earlier, represents the magnitude of the departure of the electrical response from an ideal condition and this can be determined from the location of the centre of the semicircles. Further, it is known that when α approaches zero, that is, $\{(1 - \alpha) \rightarrow 1\}$, this expression gives rise to classical Debye's formalism. Figure 6 shows the variation of real and imaginary parts of impedance (Z' and Z'', resp.) with frequency at different temperatures. It is observed that the magnitudes of both Z' and Z'' decrease with increase in frequency, thus indicating an increase in ac conductivity with rise in frequency. At temperatures <400°C, the plots (not shown in the plot for the sake of brevity) almost resemble with straight lines having large slopes, thereby indicating insulating behavior of the samples. As the temperature is increased, the slopes of the curves decrease and the curves bend down towards the abscissa, thereby indicating an increase in conductivity of the material. As shown in Figure 7(a), two semicircular arcs or depressed circular arcs are seen in the complex plane plot corresponding to a temperature of 450°C which can be explained on the basis of two parallel RC elements connected in series, one branch is associated with the grain and other with the grain boundary of the sample. The arc of grain generally lies on a frequency range higher than that of grain boundary, since the relaxation

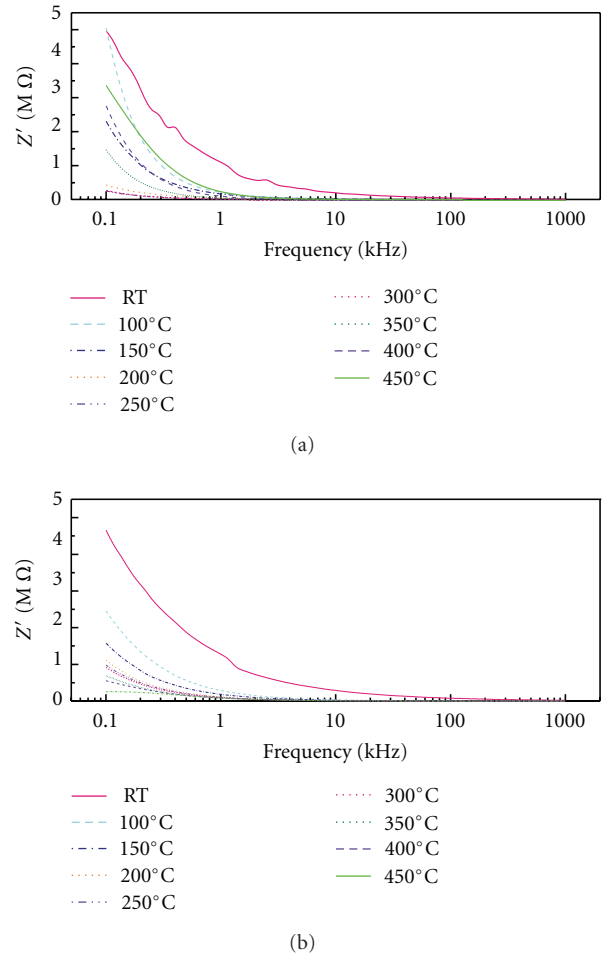

Figure 6: Frequency dependence of real and imaginary parts of the impedance of BNBT06 ceramic at the different indicated temperatures.

time $\tau(= 1/\text{fmax})$ for the grain boundary is much larger than that of the bulk crystal. This trend indicated negative temperature coefficient of resistance (NTCR) behavior of BNBT06 like that for a semiconducting material. The centers of the semicircles lie below the x-axis at an angle "ϕ" (not shown in the plots for the sake of brevity), thereby indicating non-Debye-type relaxation process in BNBT06. The observed data indicated that the conduction in BNBT06 is predominant through grain boundary and thus it gives a scope for variety of device applications for this material.

3.4.2. Modulus Spectrum Analysis. In polycrystalline materials, impedance formalism emphasizes grain boundary conduction process, while bulk effects on frequency domain dominate in the electric modulus formalism. The use of modulus spectroscopy plot is particularly useful for separating the components with similar resistance but different capacitance. The other advantage of electric modulus formalism is that the electrode effect is suppressed. Due to the above reasons, complex electric modulus formalism was also adopted in the present case in order to see the different effects

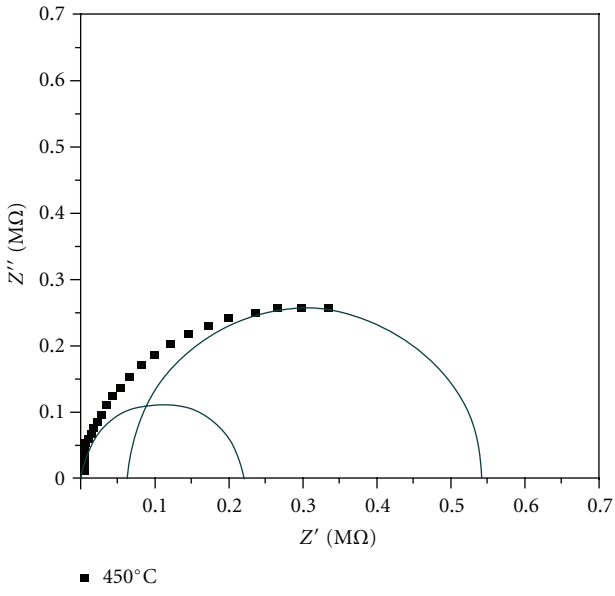

(a)

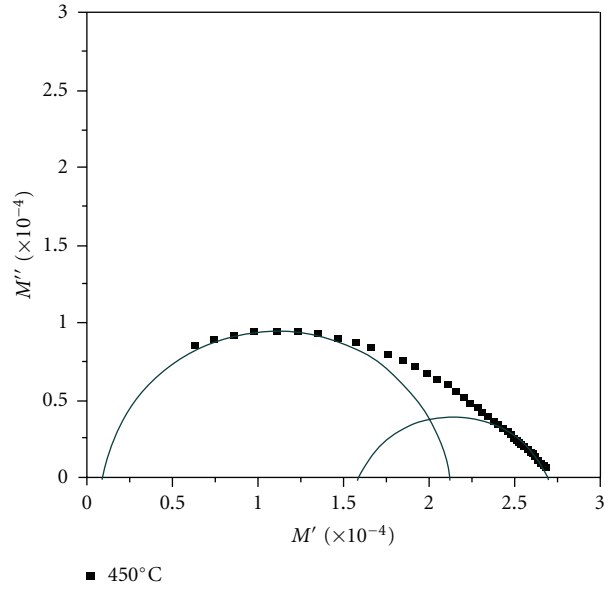

(b)

Figure 7: (a) and (b): Nyquist plots in the complex impedance and electric modulus planes, respectively, for BNBT06.

separately. Dielectric relaxation studies were carried out in the complex modulus M^* formalism. Variation of real and imaginary parts of the electric modulus (M' and M'' as a function of frequency at various temperatures) was studied. From the study, it transpired that the value of M' increases from the low frequency towards a high-frequency limit and the dispersion shifts to high frequency as temperature increases. The Nyquist plot of M'' versus M' at 450°C (Figure 7(b)) clearly revealed grain and grain-boundary peaks, thereby giving different values of $R_g(= 0.221\,M\Omega)$, $R_{gb}(= 0.543\,M\Omega)$, $C_g(= 0.621\,nF)$, and $C_{gb}(= 2.156\,nF)$. These data yield the grain and grain-boundary relaxation times equal to 0.1365 ms and 1.170 ms, respectively. Figure 8 shows the log-log plot of ac electrical conductivity (σ_{ac}) versus frequency at different temperatures. The plots show dispersion throughout the chosen frequency range. Further, the ac conductivity, in most of the materials due to localized states, is expressed by Jonscher's power law:

$$\sigma_{ac} = \sigma_o + A\omega^s, \tag{1}$$

where σ_o is the frequency-independent (electronic or dc) part of ac conductivity, $s\,(0 \le s \le 1)$ is the index, ω is angular frequency of applied ac field and $A[= \pi N^2 e^2/6k_B T(2\alpha)]$ is a constant, e is the electronic charge, T is the temperature, α is the polarizability of a pair of sites, and N is the number of sites per unit volume among which hopping takes place. Such a variation is associated with displacement of carriers which move within the sample by discrete hops of length R between randomly distributed localized sites. The term $A\omega^s$ can often be explained on the basis of two distinct mechanisms for carrier conduction: quantum mechanical tunneling (QMT) through the barrier separating the localized sites and correlated barrier hopping (CBH) over the same barrier. In these models, the exponent s is found to have two different trends with temperature and frequency. If the ac conductivity is assumed to originate from QMT, s is predicted to be temperature independent but is expected to show a decreasing trend with ω, while for CBH the value of s should show a decreasing trend with an increase in temperature. The exponent s has been found to behave in a variety of forms [18–20]. In general, the frequency dependence of conductivity does not follow the simple power relation as given above but follows a double power law [18–21] given as

$$\sigma_{ac} = \sigma_o + A\omega^{S_1} + B\omega^{S_2}, \tag{2}$$

where σ_o is the frequency-independent (electronic or dc) part of ac conductivity. The exponent $s_1\,(0 \le s_1 \le 1)$ characterizes the low-frequency region, corresponding to translational ion hopping and the exponent $s_2\,(0 < s_2 < 2)$ characterizes the high-frequency region, indicating the existence of well-localized relaxation/reorientational process [21], the activation energy of which is ascribed to reorientation ionic hopping. Further, it may be inferred that the slope s_1 is associated with grain-boundary conductivity whereas s_2 depends on grain conductivity [22]. In the jump relaxation model (JRM) introduced by Funke [18] to account for ionic conduction in solids, there is a high probability for a jumping ion to jump back (unsuccessful hop). However, if the neighborhood becomes relaxed with respect to the ion's position, the ion stays in the new site. The conductivity in the low-frequency region is associated with successful hops. Beyond the low-frequency region, many hops are unsuccessful, and as the frequency increases, more hops are unsuccessful. The change in the ratio of successful to unsuccessful hops results in dispersive conductivity. In the perovskite-type oxide materials, presence of charge traps in the band gap of the insulator is expected. The JRM suggests that different activation energies are associated with unsuccessful and successful hopping processes. The frequency

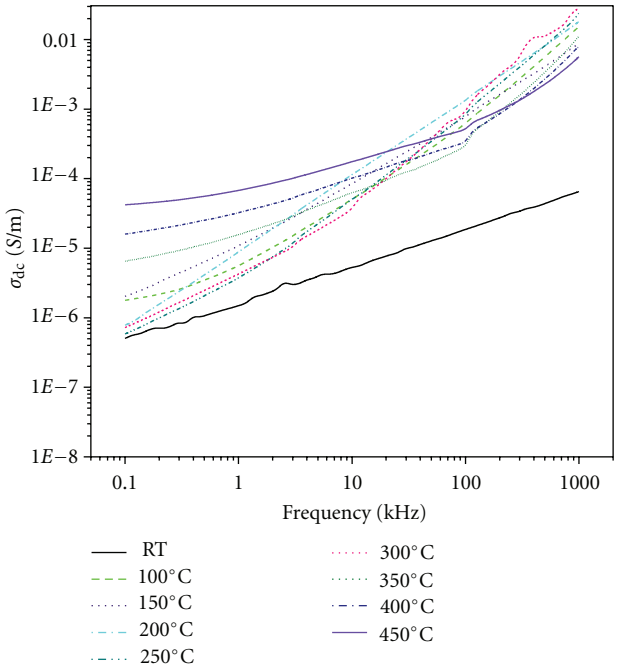

Figure 8: Variation of ac conductivity with frequency at different temperatures for BNBT06 ceramic.

and temperature dependence of ac conductivity supports hopping-type conduction in the test material. Applying JRM to the frequency response of the conductivity for the present material, it was possible to fit the data to a double power law as given in (2). The temperature-dependent variations of the exponents, s_1 and s_2, are shown in Figure 9. From the plots, it is manifested that s_1 assumes a maximum value ~1 while s_2 assumes maximum values ~1.4–1.5 with peaks appearing near T_d and T_m. The recent literature also endorsed that the exponent n (or s) is not limited to values below 1 [23].

Further, hopping conduction mechanism is generally consistent with the existence of a high density of states in the materials having band gap like that of a semiconductor. Due to localization of charge carriers, formation of polarons takes place and the hopping conduction may occur between the nearest neighboring sites. The activation energy for conduction was obtained using the Arrhenius relationship:

$$\sigma_{ac} = \sigma_o \exp\left(-\frac{E_a}{k_B T}\right). \quad (3)$$

A linear least squares fitting of the conductivity data to (3) gives the value of the apparent activation energy, E_a. Figure 10 shows the temperature-dependent ac conductivity at different frequencies and the inset shows the low- and high-temperature frequency-dependent conductivity-based activation energies of the sample. The values of E_a are found to be ~0.156 eV and ~0.512 eV in the high- and low-temperature regions, respectively, at 1 kHz and conductivity-based activation energies show a decreasing trend of variation with increasing frequency. The low value of E_a may be due to the carrier transport through hopping between localized states in a disordered manner [24, 25].

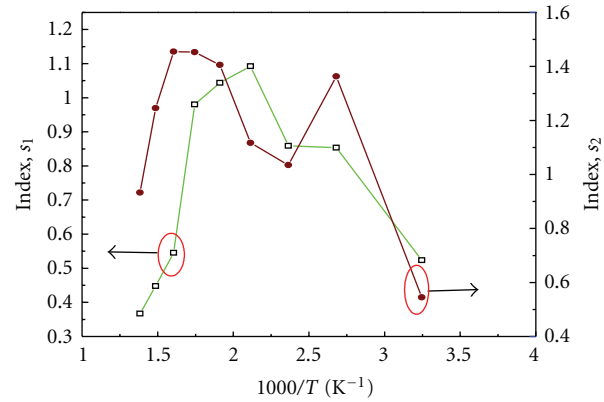

Figure 9: Temperature dependence of low- and high-frequency hopping parameters (s_1 and s_2) of BNBT06 ceramic.

The enhancement in conductivity with temperature may be considered on the basis that within the bulk, the oxygen vacancies due to the loss of oxygen are usually created during sintering and the charge compensation follows the Kröger and Vink equation [26]: $O_o \rightarrow 1/2\,O_2 \uparrow + V_o^{\bullet\bullet} + 2e^{-1}$ which shows that free electrons are left behind in the ionization process, making the materials n-type.

Based on CBH model, the minimum hopping length, R_{min} was estimated using the relation [27, 28]: $R_i = 2e^2/\pi\varepsilon\varepsilon_o W_{mi}$, where $W_{mi} = \{6k_BT/(i - s_i)\}$; $(i = 1 \text{ or } 2)$ is the corresponding binding energy. Figure 11 shows the variation of R_{min} with frequency at various temperatures. It is characterized by very low value of R_{min} in the low-frequency region, a continuous dispersion with the increase in frequency having a tendency to saturate in the high-frequency region. Such observations may possibly be related to a lack of restoring force governing the mobility of charge carriers under the action of an induced electric field. This behavior supports long-range mobility of charge carriers. On the other hand, a sigmoidal increase in the value of R_{min} with the frequency approaching ultimately to a saturation value may be attributed to the conduction phenomena due to short-range mobility of charge carriers. The *Inset* to Figure 11 presents the variation of R_{min} with temperature at the two limiting frequencies (=1 kHz and 1 MHz), showing almost exponential decay type of trends. In terms of s_1 evaluated up to 54 kHz and s_2 evaluated above 60 kHz, the values of R_{min} (R_1&R_2) were found out in the two frequency ranges. It can also be seen that the values of R_{min} decrease with increase in temperature. All the values of R_{min} were found to be ~10^{-12} m at room temperature. Thus, on an average, the value of R_{min} was found to be ~10^{-6} times smaller in comparison to the grain size of BNBT06.

Lastly, the ac conductivity data have been used to evaluate the density of states at Fermi level $N(E_f)$ using the relation [29]:

$$\sigma_{ac}(\omega) = \left(\frac{\pi}{3}\right) e^2 \omega k_B T \left\{N\left(E_f\right)\right\}^2 \alpha^{-5} \left\{\ln\left(\frac{f_o}{\omega}\right)\right\}^4, \quad (4)$$

where e is the electronic charge; f_o is the phonon frequency ($= 10^{13}$ Hz); α($= 10^{10}$ m^{-1}) is the localized wavenumber.

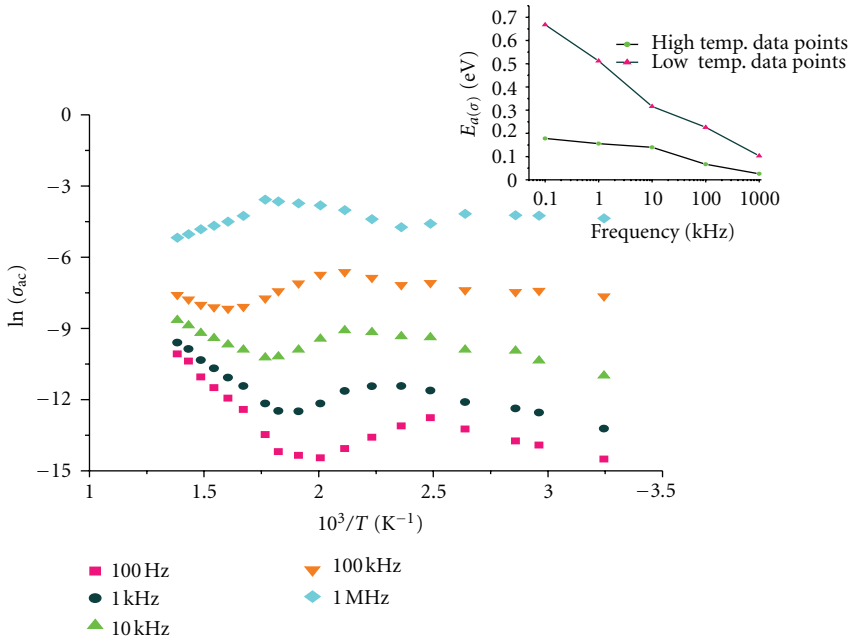

Figure 10: Temperature-dependent variation of ac conductivity at the different indicated frequencies for BNBT06 ceramic. Inset shows the low- and high-temperature frequency-dependent conductivity-based activation energies.

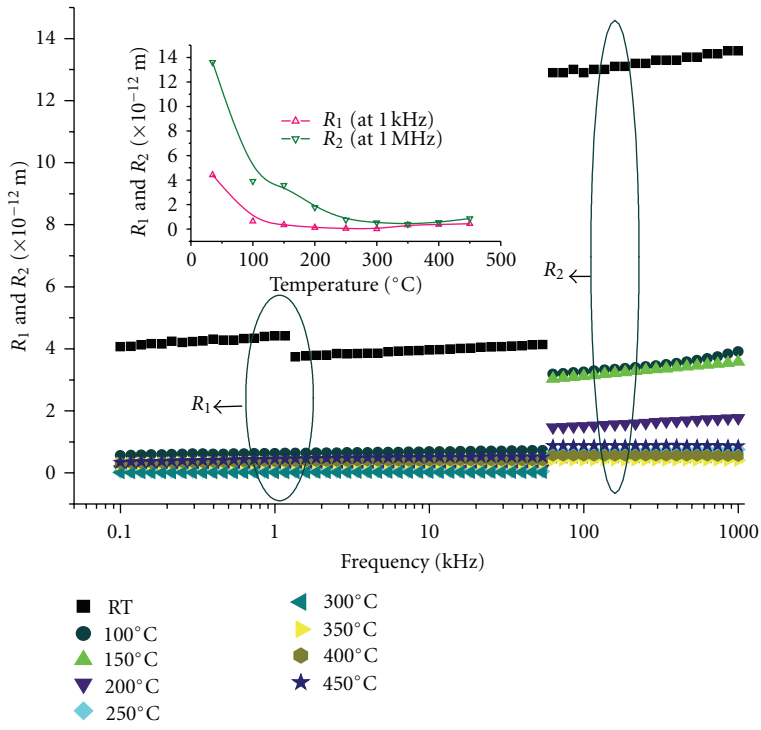

Figure 11: Frequency dependence of R_{min} of BNBT06 ceramic at different indicated temperatures. *Inset* shows the temperature dependence of R_1 at 1 kHz and R_2 at 1 MHz.

Figure 12 shows the frequency dependence of $N(E_f)$ at different temperatures. It can be seen that each of the plots shows a minimum up to 300°C after which the minimum starts disappearing and that the value of $N(E_f)$ decreases with the increasing frequency. Further, it is noted that the minima shift towards higher frequency side with the increasing value of $N(E_f)$ due to rise in temperature. The *inset* to Figure 12 shows temperature-dependent variation of $N(E_f)$ at different frequencies.The plots show peaks at and near T_d and a sharp increase beyond T_m and the anomaly is

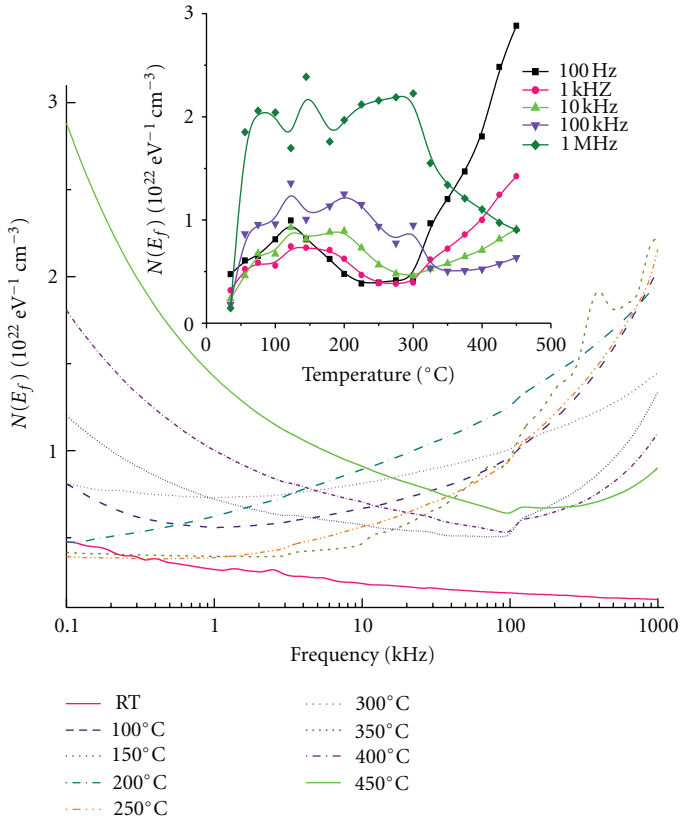

Figure 12: Frequency dependence of $N(E_f)$ of BNBT06 ceramic at different temperatures. *Inset*: temperature-dependent variation of $N(E_f)$ at different indicated frequencies.

most pronounced at 100 Hz. The reasonably high values of $N(E_f)(\sim 10^{21}\, eV^{-1}\,\text{cm}^{-3})$ suggest that the hopping between the pairs of sites dominates the mechanism of charge transport in BNBT06.

4. Conclusion

Morphotropic phase boundary composition ceramic $(Bi_{0.5}Na_{0.5})_{0.94}Ba_{0.6}TiO_3$ prepared through a high-temperature solid-state reaction method was found to have a perovskite-type structure in which both rhombohedral and tetragonal phases coexist. SEM micrograph of the sintered ceramic pellet shows dense and homogeneous packing of grains. Room temperature dielectric constant and loss factor are found to be equal to 781 and 0.085, respectively, at 1 kHz. Longitudinal piezoelectric charge coefficient (d_{33}) of the poled ceramic sample is found to be equal to 124 pC/N. The high value of dielectric constant, relatively low loss factor, and high piezoelectric charge coefficient of the test ceramic sample make this compound useful for different electronic and other sensor/actuator applications. The dielectric relaxation was found to be of non-Debye type. The frequency-dependent ac conductivity is found to obey the universal double power law. Both the pair approximation type correlated barrier hopping model and jump relaxation model are found to successfully explain the mechanism of charge transport in this substance. The minimum hopping length was found to be $\sim 10^{-6}$ times smaller in comparison to the grain size. The ac conductivity data were used to evaluate the minimum hopping length, apparent activation energy, and density of states at Fermi level.

Acknowledgment

The present work was supported by the Department of Science and Technology, New Delhi under Grant no. SR/S2/CMP-017/2008.

References

[1] Directive 2002/95/EC of European parliament and of the council of 27 January 2003 on restriction of the use of certain hazardous substances in electrical and electronic equipment, Official Journal of the European Union.

[2] T. Takenaka and H. Nagata, "Current status and prospects of lead-free piezoelectric ceramics," *Journal of the European Ceramic Society*, vol. 25, no. 12, pp. 2693–2700, 2005.

[3] G. A. Smolenskii, V. A. Isupov, A. I. Agranovskaya, and N. N. Krainik, "New Ferroelectrics of complex composition," *Soviet Physics*, vol. 2, pp. 2651–2654, 1961.

[4] J. A. Zvirgzds, P. P. Kapostins, J. V. Zvirgzde, and T. V. Krunzina, "X-ray study of phase transitions in ferroelectric $Na_{0.5}Bi_{0.5}TiO_3$," *Ferroelectrics*, vol. 40, no. 1-2, pp. 75–77, 1982.

[5] T. Takenaka, K. Sakata, and K. Toda, "Piezoelectric properties of $(Bi_{1/2}Na_{1/2})TiO_3$-based ceramics," *Ferroelectrics*, vol. 106, pp. 375–380, 1990.

[6] N. Ichinose and K. Udagawa, "Piezoelectric properties of $(Bi_{1/2}Na_{1/2})TiO_3$ based ceramics," *Ferroelectrics*, vol. 169, pp. 317–325, 1995.

[7] S.-E. Park and K. S. Hong, "Variations of structure and dielectric properties on substituting A-site cations for Sr^{2+} in $(Na_{1/2}Bi_{1/2})TiO_3$," *Journal of Materials Research*, vol. 12, no. 8, pp. 2152–2157, 1997.

[8] A. Sasaki, T. Chiba, Y. Mamiya, and E. Otsuki, "Dielectric and piezoelectric properties of $(Bi_{0.5}Na_{0.5})TiO_3(Bi_{0.5}K_{0.5})TiO_3$ systems," *Japanese Journal of Applied Physics*, vol. 38, no. 9, pp. 5564–5567, 1999.

[9] J. Suchanicz, M. G. Gavshin, A. Y. Kudzin, and C. Kus, "Dielectric properties of $(Na_{0.5}Bi_{0.5})_{1-x}Me_xTiO_3$ ceramics near morphotropic phase boundary," *Journal of Materials Science*, vol. 36, no. 8, pp. 1981–1985, 2001.

[10] B. J. Chu, D. R. Chen, G. R. Li, and Q. R. Yin, "Electrical properties of $Na_{1/2}Bi_{1/2}TiO_3$-$BaTiO_3$ ceramics ," *Journal of the European Ceramic Society*, vol. 22, no. 13, pp. 2115–2121, 2002.

[11] G. O. Jones and P. A. Thomas, "Investigation of the structure and phase transitions in the novel A-site substituted distorted perovskite compound $Na_{0.5}Bi_{0.5}TiO_3$," *Acta Crystallographica Section B*, vol. 58, no. 2, pp. 168–178, 2002.

[12] Y. Li, W. Chen, J. Zhou, Q. Xu, H. Sun, and R. Xu, "Dielectric and piezoelecrtic properties of lead-free $(Na_{0.5}Bi_{0.5})TiO_3$-$NaNbO_3$ ceramics," *Materials Science and Engineering B*, vol. 112, no. 1, pp. 5–9, 2004.

[13] J.-R. Gomah-Pettry, S. Saïd, P. Marchet, and J.-P. Mercurio, "Sodium-bismuth titanate based lead-free ferroelectric materials," *Journal of the European Ceramic Society*, vol. 24, no. 6, pp. 1165–1169, 2004.

[14] C. Peng, J. F. Li, and W. Gong, "Preparation and properties of $(Bi_{1/2}Na_{1/2})TiO_3$-$Ba(Ti,Zr)O_3$ lead-free piezoelectric ceramics," *Materials Letters*, vol. 59, no. 12, pp. 1576–1580, 2005.

[15] M. Chen, Q. Xu, B. H. Kim, B. K. Ahu, and W. Chen, "Effect of CeO_2 addition on structure and electrical properties of $(Na_{0.5}Bi_{0.5})_{0.93}Ba_{0.07}TiO_3$ ceramics prepared by citric method," *Materials Research Bulletin*, vol. 43, no. 6, pp. 1420–1430, 2008.

[16] R. Z. Zuo, C. Ye, X. S. Fang, and J. W. Li, "Tantalum doped $0.94Bi_{0.5}Na_{0.5}TiO_{3-0.06}BaTiO_3$ piezoelectric ceramics," *Journal of the European Ceramic Society*, vol. 28, no. 4, pp. 871–877.

[17] T. Gopal Reddy, B. Rajesh Kumar, T. Subba Rao, and J. Altaf Ahmad, "Structural and dielectric properties of barium bismuth titanate ($BaBi_4Ti_4O_{15}$) ceramics," *International Journal of Applied Engineering Research*, vol. 6, no. 5, pp. 571–580, 2011.

[18] K. Funke, "Jump relaxation in solid electrolytes," *Progress in Solid State Chemistry*, vol. 22, no. 2, pp. 111–195, 1993.

[19] S. R. Elliot, "A.c. conduction in amorphous chalcogenide and pnictide semiconductors," *Advances in Physics*, vol. 36, pp. 135–217, 1987.

[20] A. Pelaiz-Barranco, M. P. Gutierrez-Amador, A. Huanosta, and R. Valenzuela, "Phase transitions in ferrimagnetic and ferroelectric ceramics by ac measurements," *Applied Physics Letters*, vol. 73, no. 14, Article ID 2039, 3 pages, 1998.

[21] A. A. Youssef Ahmed, "The permittivity and AC conductivity of the layered perovskite $[(CH_3)(C_6H_5)_3P]_3HgI_4$," *Z. Naturforsch*, vol. 57, pp. 263–269, 2002.

[22] R. Rizwana, T. R. Krishna, A. R. James, and P. Sarah, "Impedance spectroscopy of Na and Nd doped strontium bismuth titanate," *Crystal Research and Technology*, vol. 42, no. 7, pp. 699–706, 2007.

[23] A. N. Papathanassiou, I. Sakellis, and J. Grammatikakis, "Universal frequency-dependent ac conductivity of conducting polymer networks," *Applied Physics Letters*, vol. 91, no. 2, Article ID 122911, 3 pages, 2007.

[24] S. Upadhyay, A. K. Sahu, D. Kumar, and O. Parkash, "Probing electrical conduction behavior of $BaSnO_3$," *Journal of Applied Physics*, vol. 84, no. 2, pp. 828–832, 1998.

[25] K. Prasad, C. K. Suman, and R. N. P. Choudhary, "Electrical characterisation of $Pb_2Bi_3SmTi_5O_{18}$ ceramic using impedance spectroscopy," *Advances in Applied Ceramics*, vol. 105, no. 5, pp. 258–264, 2006.

[26] F. A. Kröger and H. J. Vink, "Relations between the concentrations of imperfections in crystalline solids," *Solid State Physics*, vol. 3, no. C, pp. 307–435, 1956.

[27] R. Salam, "Trapping parameters of electronic defectes states in indium tin oxide from AC conductivity," *Physica Status Solidi A*, vol. 117, no. 2, pp. 535–540, 1990.

[28] M. Nadeem, M. J. Akhtar, A. Y. Khan, R. Shaheen, and M. N. Haque, "Ac study of 10% Fe-doped $La_{0.65}Ca_{0.35}MnO_3$ material by impedance spectroscopy ," *Chemical Physics Letters*, vol. 366, no. 3-4, pp. 433–439, 2002.

[29] G. D. Sharma, M. Roy, and M. S. Roy, "Charge conduction mechanism and photovoltaic properties of 1,2-diazoamino diphenyl ethane (DDE) based schottky device," *Materials Science and Engineering B*, vol. 104, no. 1-2, pp. 15–25, 2003.